

Magnetically-Guided in-Situ Microrobot Fabrication

Zhe Li, Omid Youssefi and Eric Diller

Abstract— Mobile microrobots are typically fabricated in a multi-step microfabrication process and then transported into an enclosed workspace for operation. This paper presents a new, 3D printing inspired method for in-situ fabrication of mobile magnetic microrobots with complex topology from a polymer filament on demand directly inside an enclosed operational environment. Through the use of a magnetic tip on the filament, the target shape is formed by magnetic guidance from external electromagnetic coils which wirelessly project fields into the workspace as the filament is fed through a hot needle which is inserted into the workspace. A bending model and a shape planner are developed for predicting and controlling the fabrication process. Magnetically-active millimeter-scale robotic devices of different shapes and sizes were fabricated using polylactic acid (PLA) filament with diameter as small as 50 μm . As a demonstration of the in-situ formation of a functional microrobotic device, a force-sensing microrobot with integrated sensing spring was fabricated inside an enclosed box, and then was used to measure the manipulation force during a pushing experiment by optical deformation measurement. We thus show the utility of the fabrication method for creating complex microrobot shapes remotely in enclosed environments for advanced microrobotic applications, with the potential for scaled down applications in healthcare and microfluidics.

I. INTRODUCTION

Mobile robotic devices at millimeter and smaller size scale have attracted recent interest due to their great potential in healthcare and micro-manipulation [1]. As such microrobots can be controlled wirelessly to perform tasks in small, enclosed spaces, researchers have been inspired to develop elements of their actuation, locomotion and localization. Since the functionality of microrobots in many cases depends on their shapes, fabrication of microrobots of different shapes has been a major task in this field, with most fabrication methods borrowed from the microelectromechanical systems (MEMS) community [2]. Thus, many microrobot designs have been limited to simple planar shapes which are easily defined by photolithography and other patterning methods [3-5]. Some sophisticated microrobotic structures have been made with multi-layer photolithography and silicon micromachining [6]. These microrobots contain moving spring elements and patterned magnetic material for motion and on-board tool use. Jing *et al.* [7] fabricated micro-force sensing mobile microrobots from three different materials in a process of multi-step photolithography and subsequent assembly.

The fabrication of complex 3D microrobots is even more challenging, and usually one method is only applicable for the

fabrication of one particular shape, with a focus on helical microrobots for their capability of swimming in liquid environments. Micro-wire electrical discharge machining has been used to make helical micro-swimmers from Nitinol tubing [8]. Based on a self-scrolling technique, Zhang *et al.* [9] fabricated the artificial bacterial flagella (ABF) with a helical tail of 47 μm in length. Ghosh *et al.* [10] showed a method of fabricating SiO_2 nanostructured helices 1-2 μm long using the shadow growth method (also known as glancing angle deposition). Reported by Schuerle *et al.* [11], lipidic microhelices were made by immediate metallization before the collapse of self-wrapped liposome helical tubules.

A recent method for 3D fabrication of microrobots from polymer material used multiphoton lithography, such as the helical microrobot with a microholder at one end [12] and the porous microrobot for cell culture and transportation [13]. Kobayashi *et al.* [14] have also reported a magnetically modified photocurable polymer for microstereolithography to fabricate arbitrary 3D magnetic microstructures.

Most microrobotic applications involve deployment into inaccessible spaces such as microfluidic channels and human body. The deployment will likely be done using a hypodermic needle [15, 16], limiting the dimension of the microrobots to the size of the needle gauge, resulting in overly simple and thin small geometries.

In all of these prior microrobot fabrication methods, either the fabrication process is very complex or the microrobot shape is limited. In either case, the microrobots have to be transported into their workspace after fabrication for further applications, increasing the difficulty and complexity of the operation. Here we introduce a new method for fabricating microrobots with complex shapes in-situ using filament of thermoplastic materials in a simple and rapid process. With the initial idea borrowed from fused filament-based 3D printing, the microrobot can be fabricated in-situ by bending a polymer filament as it is fed through a needle which is inserted into the workspace. Almost any arbitrary 3D wireframe shapes can be created except for some minor limitations. Even if the target workspace is inaccessible and enclosed, the fabrication can be performed directly inside the workspace by inserting a thin needle into it. No further transportation of the microrobot is required, and although the diameter of the filament cannot exceed the inner diameter of the needle, the overall microrobot shape is not constrained by the needle gauge.

We also show in this paper a bending model of the heated polymer filament with a magnet tip under magnetic guidance, and a fabrication planner for creating any desired shape through computer vision detection. The creation of several

*Research supported by the NSERC Discovery Grants Program.

The authors are with the Department of Mechanical and Industrial Engineering, University of Toronto, Toronto, ON, Canada M5S 3G8 (email: ediller@mie.utoronto.ca).

different microrobotic shapes are shown to demonstrate the dexterity of this method and its potential for being scaled down. A spring-shaped microrobot is also fabricated and then controlled as a proof of in-situ formation of a functional microrobot for applications in constrained inaccessible spaces.

II. CONCEPT

In this section, we introduce the new concept of magnetically-mediated injectable microrobot fabrication. In this method, the microrobot is fabricated by bending a polymer filament into a desired shape as it is fed through a needle which has been injected into the workspace. This method is similar to a fused filament-based 3D printing system, where a thermoplastic polymer filament is extruded from a hot moving needle and hardens as it emerges. However, in our case, the needle is stationary, and the formed filament shape rotates itself to create the target microrobot. As shown conceptually in Fig. 1, the filament is bent under torques induced by a small magnet embedded at the end of the filament under the influence of magnetic fields generated by electromagnetic coils far from the workspace. The use of magnetic fields allows the actuating coils to generate a torque on the tip of the filament in a wireless, safe and controllable manner. To induce permanent plastic deformation in the filament at the region immediately past the tip of the needle, the needle is heated to soften the filament. When the temperature of the filament is above its glass transition temperature (T_g), guided by the magnetic torque, plastic deformation will occur in a small region past the needle, which we term the plastic deformation zone (PDZ). The filament will cool down as it is fed through the needle, so the PDZ only consists of the region with temperature above T_g . The cooled region of filament outside the PDZ is not plastically deformed by the magnetically applied bending moment, and is thus treated as a formed rigid structure of the microrobot. By continuously feeding the filament through the needle and correspondingly changing the applied magnetic field, a microrobot of a desired shape can be formed.

III. MODELLING AND CHARACTERIZATION

In this section, we introduce a theoretical model of filament bending mechanics under magnetic influences, and a magnet angle planner. We will later use these tools to predict and control the fabrication process.

A. Bending Mechanics

During the fabrication process, the filament is bent at the PDZ by a bending moment provided by the magnetic torque induced on the magnet at the end of the filament. Given a tip magnet with magnetic moment \vec{m} , the torque \vec{T} under an applied field \vec{B} is given by

$$\vec{T} = \vec{m} \times \vec{B}. \quad (1)$$

The torque acts to align the magnet with the applied field, and is at the maximum value when the applied field is perpendicular to the magnetization direction. Due to the cross product in (1), no torque can be generated about the

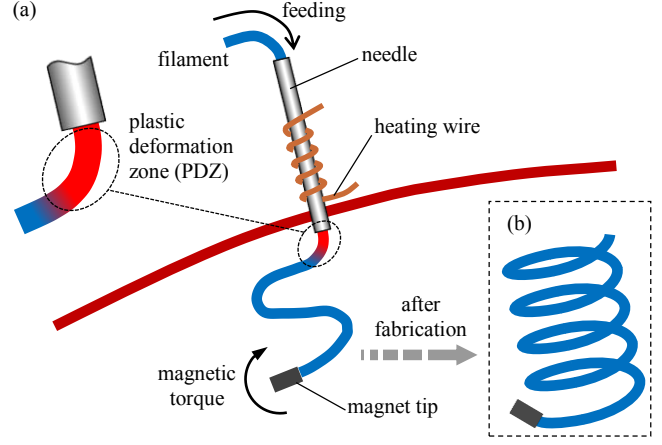


Figure 1. Conceptual schematic of the in-situ microrobot fabrication system. (a) Components and setup of the fabrication system, showing the injection fabrication of a 3D shape inside an enclosed environment. (b) An example of target microrobot shape possible through the fabrication process.

magnetization axis, which will result in a limitation during the fabrication of some shapes.

For a microrobot fabricated from a continuous filament, we introduce two fundamental shape elements, the sharp angle and the continuous arc, which can be fabricated by two types of bending control developed here, the discrete bending and the continuous bending.

In the discrete bending case, shown in Fig. 2(a), the filament is first fed through the needle for a desired length at a temperature lower than T_g to attain a straight line segment, then the needle is heated to above T_g and a magnetic field is applied to bend the filament by a desired angle α .

As bending happens over the length of PDZ (l_{PDZ}), there will always be a curved part in the PDZ, and the minimum radius of the curved part is the radius R of the filament (Fig. 2(b)). This indicates that l_{PDZ} will affect the accuracy of a discrete bend when approximated as a sharp angle. According to the preliminary heat transfer simulation (results outside the scope of this work), the heat transfer along the filament will reach equilibrium within 2 seconds, and the final l_{PDZ} is of the same order of magnitude as the radius of the filament, suggesting that the radius of a discrete bend is negligible for a sharp angle.

In the continuous bending case, shown in Fig. 2(c), to induce a constant curvature along the length of the filament, the magnetic field is applied to rotate the magnet at a constant rate while the filament is constantly fed through the heated needle. The angular changing rate $\dot{\alpha}$ of the magnet angle is dictated by the feeding speed v of the filament and the desired curvature κ of the arced filament, governed as

$$\dot{\alpha} = v\kappa. \quad (2)$$

The mechanics of the bending is mainly governed by the magnitude of the applied magnetic field, the magnetic moment of the magnet tip and the gravity of the magnet tip. Theoretical analysis reveals that for a vertical needle setup, the bending angle α can be approximated from torque balance as

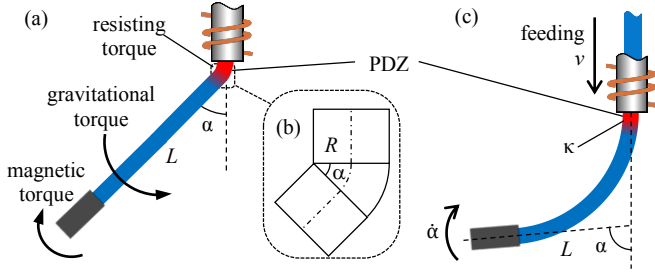


Figure 2. Types of bending. (a) Discrete bending. (b) Minimum radius of discrete bending. (c) Continuous bending.

$$\vec{\tau}_B = \vec{\tau}_g + \vec{\tau}_R(d, \alpha, T_y, \dots), \quad (3)$$

where $\vec{\tau}_B$ is the magnetic torque, $\vec{\tau}_g$ is the gravitational torque, and $\vec{\tau}_R$ is the resisting torque due to polymer creep and environmental resistances. The $\vec{\tau}_R$ term depends on the diameter of the filament d , bending angle α , and the temperature at the PDZ T_y , along with other parameters that are complex to model, and here we assume this torque to be small. Assuming an orthogonal external field with respect to the magnetization direction of the magnet, $\vec{\tau}_B$ can be replaced by mB , where m is the magnitude of the magnetic moment of the magnet. Similarly, $\vec{\tau}_g$ can be replaced by $m_0 g L \sin \alpha$, where L , for the discrete bending case, is the distance from the center of the magnet with mass m_0 to the tip of the needle, and for continuous bending L is the distance from the center of the magnet to the axis of the needle along the direction of the magnet. Assuming the resisting torque $\vec{\tau}_R$ to be zero gives a bending angle of

$$\alpha = \arcsin\left(\frac{MB}{\rho g L}\right), \quad (4)$$

where M is the volume magnetization of the magnet, B is the magnitude of the orthogonally applied magnetic field, ρ is the density of the magnet, and g is the gravitational acceleration. Thus, it can be seen that with effect of gravity present, the bending angle α is only dependent on the bending length L and the material properties of the magnet. This indicates that the size of the filament and its magnet tip can be reduced with no effect on the achievable bend angles, implying that the presented fabrication method will scale well to smaller magnet and filament sizes. To get accurate bending in fabrication, the bending angle is controlled by detecting the heading of the magnet tip through computer vision.

B. Magnet Angle Planner

During the fabrication process, as the filament is fed through the needle, the already-formed part of the microrobot will rotate itself into a desired shape, and the heading of the magnet tip will change along with the rotation of the structure. Thus, by tracking and controlling the heading of the magnet α during the feeding of the filament, the fabrication process can be controlled and the final shape of the microrobot will be fabricated as desired. Here a magnet angle planner is developed, such that the magnet angle α is pre-planned as a function of the length S of the filament that has been fed through the needle for any desired shape.

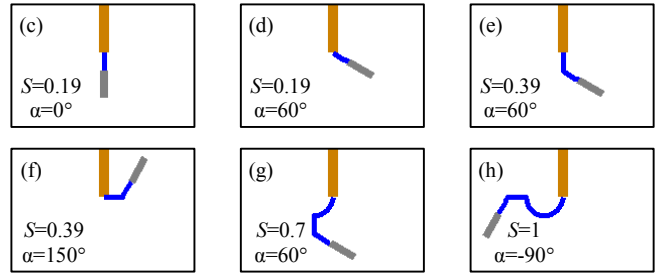
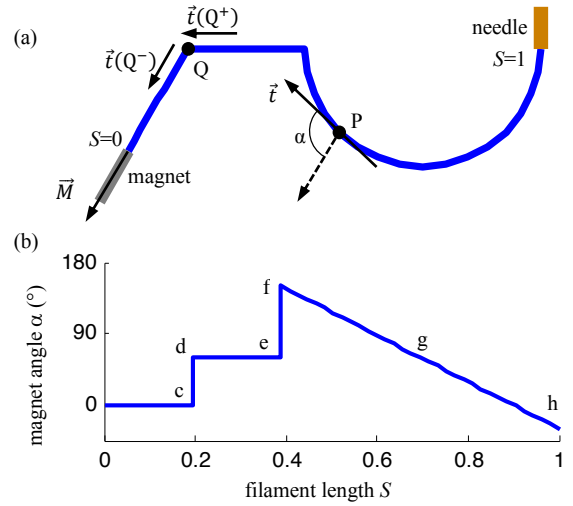


Figure 3. Magnet angle planner. (a) Geometric model of the magnet angle planner. (b) The desired magnet angle from $S=0$ to $S=1$ for the shape shown in (a). (c)-(h) Key frames of fabrication simulation for the desired shape shown in (a). The filament length S and magnet angle α are shown in each frame. (c)-(h) correspond to points c-h in (b).

The magnet angle α is measured with respect to the axis of the needle, which is vertically fixed during the fabrication process. For any point P along the length of the desired shape, when that point appears at the tip of the needle during the fabrication, the needle is also pointing at the direction of the tangent vector \vec{t} of that point. Thus the magnet angle α for a point P can be measured as the angle between the heading of the magnet \vec{M} and the tangent vector \vec{t} of that point (Fig. 3(a)). The corresponding filament length S is the length of the filament between the magnet tip and that point.

A discontinuous point in the magnet angle planner occurs in the case of a sharp angle in a desired shape, where a tangent line does not exist at the vertex Q of the angle, as shown in Fig. 3(a). This corresponds to a discrete bend in the shape, where the filament length S is not changing while the magnet angle will jump from the value of before the bend ($S=Q^-$) to that of after the bend ($S=Q^+$), as shown at points c and d in Fig. 3(b).

Following the same principle, this magnet angle planner could easily be extended to a 3D shape, with the heading of the magnet being described by two angles in 3D.

IV. RESULTS AND DISCUSSION

A. Fabrication System: Magnetic Field and Extrusion

The magnetic fields for fabrication and subsequent motion

control of microrobots are generated using a custom magnetic coil system, shown in Fig. 4(a)-(b). The prototype coil system is composed of two pairs of orthogonal Helmholtz coils and can generate a uniform magnetic field of up to 14 mT in a vertical plane over a workspace of $6.75 \times 3.50 \times 9.43$ (cm), and at frequencies up to 120 Hz. The field produced by each coil is proportional to the current through the coil, which is controlled by amplifiers (ADVANCED Motion Controls, 30A8) and directed by an analog output card (SENSORAY, Model 826) from a custom Linux-based C-code PC control software. The feeding of the filament is controlled by a custom filament feeder driven by a stepper motor as shown in Fig. 4(c)-(d). The needle is heated by resistance wire wrapped around the needle as shown in Fig. 4(d), and the temperature is measured by a thermocouple, and feedback control of the needle temperature is performed along for automated fabrication. A camera (FOculus, FO124TB) is mounted to the side of the coil system to detect the magnet angle. To simulate the enclosed environment of in-situ fabrication for medical, microfluidic or microfactory applications, an acrylic box is placed inside the coil system with only a small hole for access, and all microrobot fabrication must thus be performed inside the box.

Among thermoplastic materials, polylactic acid (PLA) was selected as the fabrication material due to its low T_g (56°C) and its semi-crystalline structure, which ensures a uniform thermal property along the filament and makes the fabrication process more predictable.

PLA filament of $200\ \mu\text{m}$ in diameter was pre-fabricated using a custom hot extrusion method from 1.75 mm filament intended for use in 3D printing. In this pre-fabrication, the filament was extruded at 225°C through an extrusion nozzle of inner diameter $200\ \mu\text{m}$, at an input rate of $0.45\ \text{mm/s}$. As thinner filament was extruded from the hot end, it cooled down and then hardened immediately. Extrusion was done vertically and therefore the filament was pulled by its own weight, creating a uniform diameter along the filament. Unlike filaments readily available for purchase, negligible residual stress was present in this filament, which is necessary for use in the fabrication of microrobots.

B. Microrobot Fabrication Experiments

To demonstrate the effectiveness of the in-situ fabrication method with custom produced filaments, as shown in Fig. 5, different shapes containing both discrete and continuous bending were made using the pre-fabricated PLA filament. The magnet tip used were two cylindrical neodymium magnets ($\Phi 0.75 \times 1\ \text{mm}$) stacked together, and was manually glued to the end of the filament. All the demonstrated shapes were fabricated in less than three minutes, and the process can be made faster by increasing the filament feeding speed and tuning the parameters of the magnet angle controller.

To show the potential of the fabrication method at a smaller scale, a microscale “S”-shaped device was fabricated, as shown in Fig. 5(k). The filament used in this demonstration was fabricated to be $50\ \mu\text{m}$ in diameter using the hot extrusion method, and the magnet tip was a cube magnet of side length

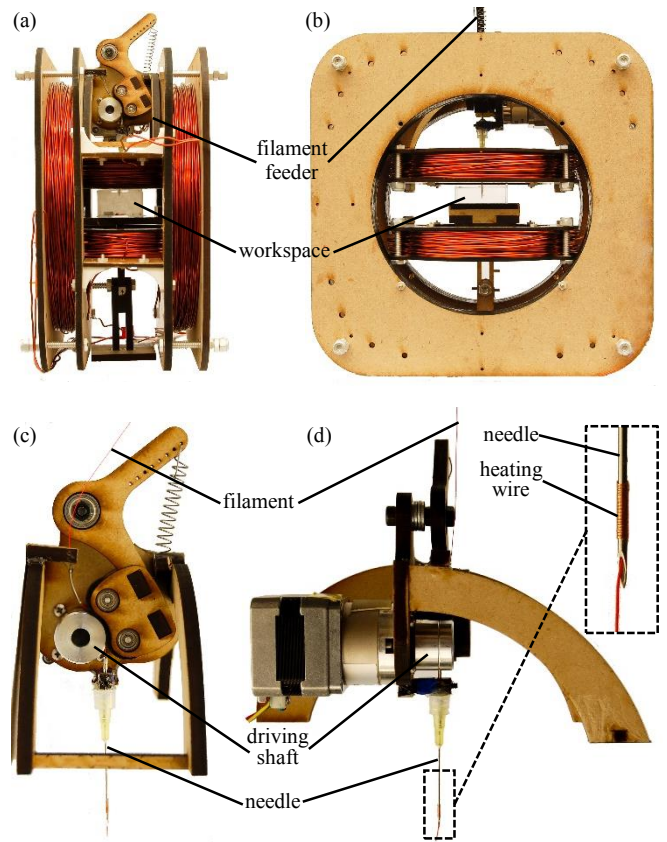


Figure 4. Prototype of magnetic in-situ microrobot fabrication system. (a)-(b) Side view and front view of the coil system. The filament feeder is placed on the coil system, the tip of the needle is in the center of the coil system and is inside the acrylic box. The dimension of the box is $40 \times 40 \times 20$ (mm), and the diameter of the access hole is $4.5\ \text{mm}$. (c)-(d) Side view and front view of the filament feeder. The filament is fed through the needle by the driving shaft attached to the shaft of the stepper motor. The detail of the tip of the needle with heating wire wrapped around is shown in the inset of (d).

$250\ \mu\text{m}$. However, as the filament is much thinner than the inner diameter of the needle, the sharpness of the discrete bending was affected. The feeding mechanism no longer worked perfectly with the filament as it was much thinner and more flexible, affecting the length accuracy of each segment. Future work will focus on the fabrication with higher accuracy at the microscale.

The averaged shape deviation D_{avg} is used to characterize the accuracy of the fabricated shape. To calculate D_{avg} , the morphological skeleton of the fabricated shape was extracted and superimposed on the desired shape. By changing the relative position and orientation of the two shape curves, a minimum area A_{min} of the space enclosed by the two curves was found and calculated. The area A_{min} was then normalized to the length of the desired shape to form D_{avg} . For the “S” shaped microrobot shown in Fig. 5(b), D_{avg} is within $250\ \mu\text{m}$, which shows a high accuracy compared to the size of the fabricated shapes that is in millimeter scale.

C. Functional Microrobot Demonstration

As an example of in-situ fabrication of a functional microrobot with a complex shape that is integral to its task,

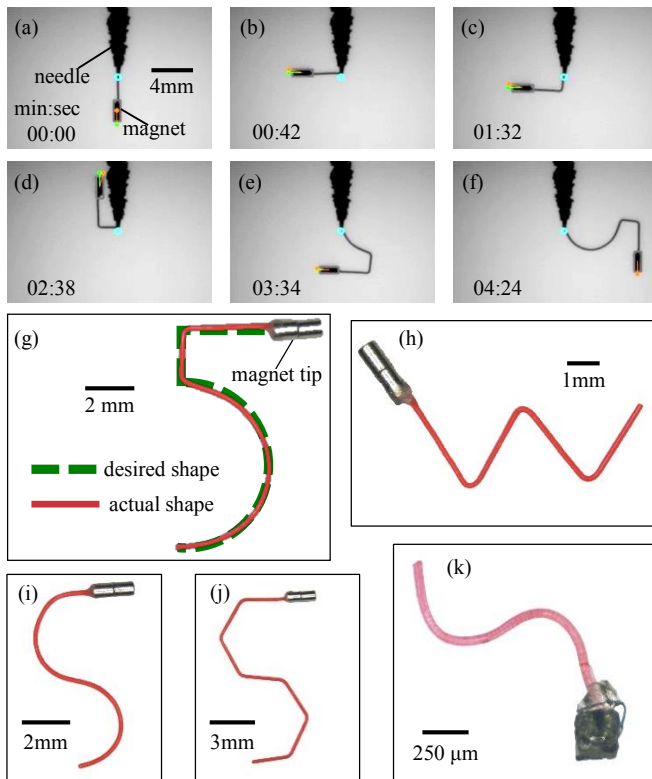


Figure 5. Fabricated microrobots of different shapes. (a)-(f) key frames of the fabrication process of a “5”-shaped microrobot in chronological order. (g) The comparison between the actual shape and the desired shape of the microrobot. (h)-(j) Demonstration of a “W”-shaped microrobot from three 120 ° discrete bends, an “S”-shaped microrobot from two 180 ° arcs, an “S” shaped microrobot from six 60 ° discrete bends. (k) Smaller scale microrobot with filament of diameter 50 μm ; super glue for attaching the cube magnet is visible here. Fabrication is shown in supplementary video.

we produced a micro-spring (spring-shaped microrobot) inside the enclosed acrylic box with force feedback capability when performing manipulations, as was demonstrated in [7]. The force-sensing microrobot was then magnetically controlled to push a small aluminum nut, during which the pushing force was measured. Three stacked cylindrical neodymium magnets ($\Phi 1 \times 1$ mm) were used as the magnet tip for fabrication. The magnet tip was then used to control the movement of the microrobot and to apply a magnetic pushing force. The pushing force can be measured by optically detecting the deformation of the calibrated force-sensing microrobot. As shown in Fig. 6(c)-(h), we fabricated the microrobot in-situ, released it from the needle, moved it into position using magnetic gradient pulling, and magnetically actuated it to apply the pushing force. All of these tasks, except for the release of the device, were performed inside the small enclosed acrylic box without direct human interference.

To calibrate the stiffness of the force-sensing microrobot for force measurement, three micro-springs with the same shape as the microrobot were fabricated separately. A micro-force sensor (FemtoTools, FT-RS1002) was used to calibrate the stiffness of the micro-springs. As shown in Fig. 6(a), the probe of the micro-force sensor was flush with the tip of the micro-spring for the purpose of taking a force-displacement measurement. As shown in Fig. 6(a), the three pre-fabricated

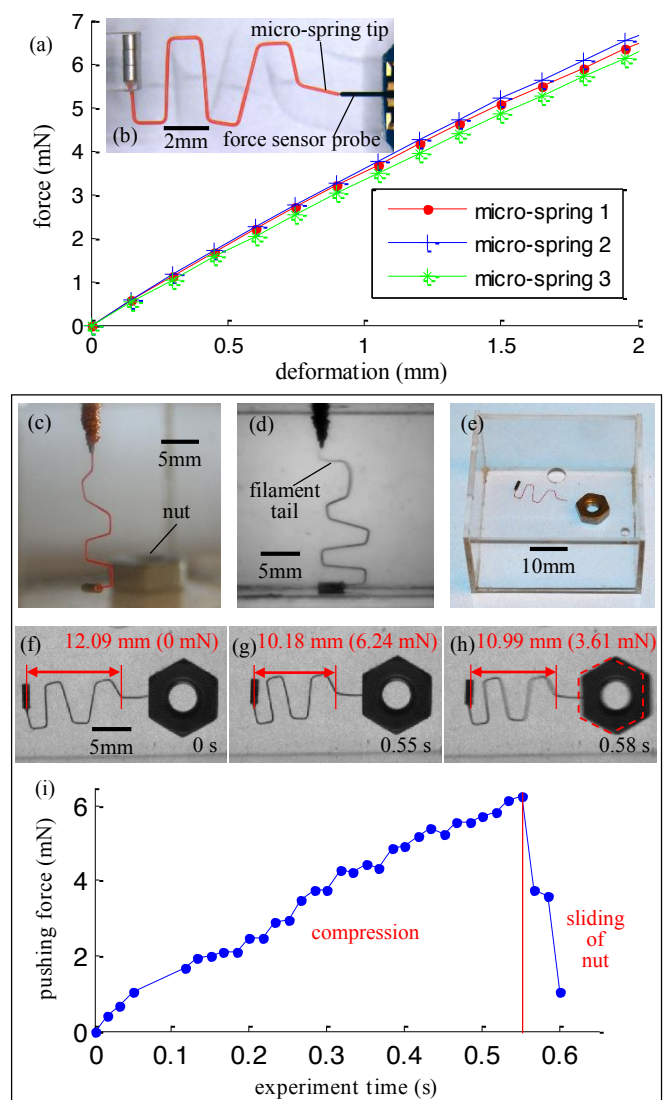


Figure 6. Stiffness calibration, in-situ fabrication, release, motion control and force measurement of a force-sensing microrobot. (a) Force vs. deformation plot of the three pre-fabricated force-sensing microrobots. (b) Calibration setup of the force-sensing microrobot. (c) Fabricated force-sensing microrobot before released from the needle. (d) Force-sensing microrobot was released from the needle by the application of an oscillating field. (e) The released force-sensing microrobot and pre-placed nut inside the box. (f) Beginning of the pushing experiment when the force-sensing microrobot was at its original length. (g) The force-sensing microrobot was compressed to reach its maximum deformation just before the nut was pushed to move. (h) The deformation of the force-sensing microrobot was smaller during the motion of the nut. The red dotted line is the original position of the nut. (i) Pushing force vs. experiment time during a complete pushing of the nut. The time stamps in (f)-(h) corresponds to the time in x axis. Experiment is shown in supplementary video.

micro-springs have very similar stiffness (3.28 N/m, 3.37 N/m and 3.16 N/m), which indicates that the force-sensing microrobot can be fabricated with a known stiffness. The stiffness used for the in-situ force-sensing microrobot was the average stiffness of the three micro-springs, 3.27 N/m.

A nut was placed inside the box prior to the fabrication of the force-sensing microrobot. In order to release the microrobot from the needle, the needle was heated to 150 °C and an oscillating magnetic field was applied, such that the

device oscillated itself to stretch and thin the filament at the tip of the needle until it breaks (Fig. 6(d)). The cut tip of the microrobot had a long thin filament tail as it was broken off by stretching the filament. This tail is undesirable for use as a pushing tip, so we manually cut off the thin tail after it was released. A better method for releasing the device without direct human interference will be investigated in future work. The released microrobot was then controlled by gradient pulling using a permanent magnet in order to push the microrobot against the nut inside the box (Fig. 6(e)). The original length of the micro-spring was 12.09 mm (Fig. 6(f)), and was compressed to 10.18 mm at its maximum deformation just before the nut was moved, which corresponds to a force of 6.24 mN (Fig. 6(g)). After the nut began to move, the force reduced to zero as the nut accelerated first and then decelerated. The pushing force during the whole pushing process is shown in Fig. 6(i). In the current vision system, one pixel represents an actual length of 99 μm and gives a force resolution of 0.32 mN.

V. CONCLUSION

The new fabrication method presented in this paper has the potential to simplify the fabrication process of existing microrobots, and also creates the possibility of fabricating more complex 3D microrobot shapes for advanced functionalities. In addition, the process of transporting the microrobot from a fabrication system into its workspace is no longer a problem as the microrobot is directly fabricated in-situ through an injection needle. This allows for reduction of the size of the access hole to the diameter of the injection needle, and facilitates further operation of the microrobot.

Due to the limitation that no magnetic torque can be generated about the magnetization axis of the magnet, only planar shapes are demonstrated in this paper. In a 3D fabrication the PDZ behaves kinematically as a spherical joint with 3 degrees of freedom (DOF), while the magnetic torque can only be applied about two axes of the magnet. The gravitational torque of the magnet will usually work on the third axis for most 3D shapes, causing the system to be underactuated and out of control. In future work, this limitation could be improved by applying magnetic force compensation to fully actuate the system.

Although microrobots with complex shapes can be fabricated in-situ rapidly and accurately using this method, the target shape is not completely arbitrary. The magnet or the formed rigid part of the microrobot may hit the injection needle during the fabrication of certain shapes, such as a shape with closed curves, limiting the capability of this method. A further characterization of the shape creation potential of the method will be studied.

To make the method more applicable in real applications like healthcare and microfluidics, the size of the fabricated microrobot needs to be further scaled down, so even thinner filaments should be fabricated. Filament of diameter 10 μm can be fabricated using the current hot extrusion method, but the mechanism for feeding thinner filaments should also be investigated. Methods of softening the filament in a bend and

breaking the filament off to release the fabricated microrobot at a lower temperature should also be explored to avoid any burn damage to the workspace. As a potential method for removing the microrobot after the tasks are finished, the micro-device could be controlled to move out of its workspace through the heated injection needle as it straightens itself, which works like a reversed fabrication process of the microrobot.

REFERENCES

- [1] K. E. Peyer, L. Zhang and B. J. Nelson, "Bio-inspired magnetic swimming microrobots for biomedical applications," *Nanoscale*, vol. 5, no. 4, pp. 1259-1272, 2013.
- [2] E. Diller and M. Sitti, "Micro-Scale Mobile Robotics," *Found. and Trends in Robotics*, vol. 2, no. 3, pp. 143-259, 2011.
- [3] E. Diller, S. Floyd, C. Pawashe and M. Sitti, "Control of Multiple Heterogeneous Magnetic Microrobots in Two Dimensions on Nonspecialized Surfaces," *IEEE Trans. Robot.*, vol. 28, no. 1, pp. 172-182, 2012.
- [4] W. Jing, N. Pagano and D. J. Cappelleri, "A novel micro-scale magnetic tumbling microrobot," *Micro-Bio Robot*, vol. 8, no. 1, pp. 1-12, 2013.
- [5] M. S. Sakar, E. B. Steager, D. H. Kim, A. A. Julius, M. Kim, V. Kumar and G. J. Pappas, "Modeling, control and experimental characterization of microbiorobots," *Int. J. Robotics Res.*, vol. 30, no. 6, pp. 647-658, 2011.
- [6] D. R. Frutiger, K. Vollmers, B. E. Kratochvil and B. J. Nelson, "Small, Fast, and Under Control: Wireless Resonant Magnetic Micro-agents," *Int. J. Robotics Res.*, vol. 29, no. 5, pp. 613-636, 2009.
- [7] W. Jing and D. J. Cappelleri, "Micro-Force Sensing Mobile Microrobots," *Proc. of SPIE*, vol. 9494, 2015.
- [8] A. W. Mahoney, J. C. Sarrazin, E. Bamberg and J. J. Abbott, "Velocity Control with Gravity Compensation for Magnetic Helical Microswimmers," *Adv. Robotics*, vol. 25, no. 8, pp. 1007-1028, 2011.
- [9] L. Zhang, J. J. Abbott, L. Dong, B. E. Kratochvil, D. Bell and B. J. Nelson, "Artificial bacterial flagella: Fabrication and magnetic control," *Appl. Phys. Lett.*, vol. 94, no. 6, 064107, 2009.
- [10] A. Ghosh and P. Fischer, "Controlled Propulsion of Artificial Magnetic Nanostructured Propellers," *Nano Lett.*, vol. 9, no. 6, pp. 2243-2245, 2009.
- [11] S. Schuerle, S. Pané, E. Pellicer, J. Sort, M. D. Baró and B. J. Nelson, "Helical and Tubular Lipid Microstructures that are Electroless-Coated with CoNiReP for Wireless Magnetic Manipulation," *Small*, vol. 8, no. 10, pp. 1498-1502, 2012.
- [12] S. Tottori, L. Zhang, F. Qiu, K. K. Krawczyk, A. Franco-Obregón and B. J. Nelson, "Magnetic Helical Micromachines: Fabrication, Controlled Swimming, and Cargo Transport," *Adv. Mater.*, vol. 24, no. 6, pp. 811-816, 2012.
- [13] S. Kim, F. Qiu, S. Kim, A. Ghanbari, C. Moon, L. Zhang, B. J. Nelson and H. Choi, "Fabrication and Characterization of Magnetic Microrobots for Three-Dimensional Cell Culture and Targeted Transportation," *Adv. Mater.*, vol. 25, no. 41, pp. 5863-5868, 2013.
- [14] K. Kobayashi and K. Ikuta, "Three-dimensional magnetic microstructures fabricated by microstereolithography," *Appl. Phys. Lett.*, vol. 92, no. 26, 262505, 2008.
- [15] M. P. Kummer, J. J. Abbott, B. E. Kratochvil, R. Borer, A. Sengul and B. J. Nelson, "OctoMag: An Electromagnetic System for 5-DOF Wireless Micromanipulation," *IEEE Trans. Robot.*, vol. 26, no. 6, pp. 1006-1017, 2010.
- [16] G. Chatzipirpiridis, O. Ergeneman, J. Pokki, F. Ullrich, S. Fusco, J. A. Ortega, K. M. Sivaraman, B. J. Nelson and S. Pané, "Electroforming of Implantable Tubular Magnetic Microrobots for Wireless Ophthalmologic Applications," *Adv. Healthc. Mater.*, vol. 4, no. 2, pp. 209-215, 2015.